Received: 17 October 2018 | Revised: 1 February 2019 | Accepted: 6 February 2019

DOI: 10.1002/bit.26955

ARTICLE

WILEY BIOTECHNOLOGY AND BIOENGINEERING

Modeling, simulations, and optimization of smooth muscle cell tissue engineering for the production of vascular grafts

Yahya Elsayed[1,2] | Constantina Lekakou[1] | Paul Tomlins[3]

[1]Department of Mechanical Engineering Sciences, Engineering Materials Centre, University of Surrey, Guildford, Surrey, UK

[2]Department of Mechanical Engineering Sciences, Centre of Biomedical Engineering, University of Surrey, Guildford, Surrey, UK

[3]National Physical Laboratory, Teddington, Middlesex, UK

Correspondence
Constantina Lekakou, Engineering Materials Centre, University of Surrey, Guildford, Surrey GU2 7XH, UK.
Email: C.Lekakou@surrey.ac.uk

Abstract

The paper presents a transient, continuum, two-phase model of the tissue engineering in fibrous scaffolds, including transport equations for the flowing culture medium, nutrient and cell concentration with transverse and in-plane diffusion and cell migration, a novel feature of local in-plane transport across a phenomenological pore and innovative layer-by-layer cell filling approach. The model is successfully validated for the smooth muscle cell tissue engineering of a vascular graft using crosslinked, electrospun gelatin fiber scaffolds for both static and dynamic cell culture, the latter in a dynamic bioreactor with a rotating shaft on which the tubular scaffold is attached. Parametric studies evaluate the impact of the scaffold microstructure, cell dynamics, oxygen transport, and static or dynamic conditions on the rate and extent of cell proliferation and depth of oxygen accessibility. An optimized scaffold of 75% dry porosity is proposed that can be tissue engineered into a viable and still fully oxygenated graft of the tunica media of the coronary artery within 2 days in the dynamic bioreactor. Such scaffold also matches the mechanical properties of the tunica media of the human coronary artery and the suture retention strength of a saphenous vein, often used as a coronary artery graft.

KEYWORDS

modeling, simulations, smooth muscle cells, tissue engineering, vascular grafts

1 | INTRODUCTION

Tissue engineering (TE) of arteries is a complex field encompassing interlinked materials and processes, including the scaffold, the cells and their attachment, growth, migration and death, feeding, nutrient transport and utilization, and extracellular matrix (ECM) formation (Dzobo et al., 2018). As these processes evolve in parallel, modeling and computational simulations are essential for the interpretation of experimental results, determination of the dominating factors, design, and optimization of the scaffold and the TE technique.

Cells require different nutrients to survive that may be simplified to two main and critical ones, oxygen and glucose. The study of the transport of these nutrients is a common field of research in tissue engineering. Initial numerical models considered the only diffusion of nutrients through a homogeneous, single-phase continuum (Croll et al., 2005; Pierre, Gemmiti, Kolambkar, Oddou, & Guldberg, 2008; Sengers, Van Donkelaar, Oomens, & Baaijens, 2005), which would be applicable to nonporous solid or gel-type of substrates, and, in fact, have also been used to determine the diffusion coefficient of nutrients through specific gel materials (Elsayed, Lekakou, & Tomlins, 2014). For porous scaffolds, given that the nutrients are dissolved or dispersed in the culture medium, their transport is governed by the convection and permeation of the culture medium through the scaffold to the cells, the diffusion, and uptake of nutrients. Under static conditions, due to the instantaneous permeation of the culture medium in the pore channels so that the nutrient concentration in the pores reaches steady state, the diffusion process still governs the transport of nutrients, as diffusion is slow and makes difficult for cells to survive if they are a few hundred micrometers away from the surface in contact with the culture medium (Rouwkema & Khademhosseini, 2016; Skrzypek et al., 2018; Stamatialis, 2017). Dynamic bioreactors use convection and forced permeation through porous scaffolds to facilitate and accelerate

the transport of nutrients (experimental studies by Daly, Sathy, & Kelly, 2018; Nguyen, Ko, Moriarty, Etheridge, & Fisher, 2016), in which case, full transport models including the convection and permeation terms, as well as diffusion, are required and are incorporated in this study.

Cell growth leads to the population of scaffold and blocking of pores that result in the reduction and ultimately the inhibition of the transport of nutrients, which will accelerate the death of cells. The aim of an optimized tissue engineering process is (a) to complete the scaffold population by cells before the nutrient concentration falls below the survival threshold; (b) to achieve tissue formation in the shortest possible time period for economic reasons and supply readiness of the vascular graft; (c) to achieve the required rate of ECM production and tissue formation that compensates any degradation of the scaffold in a timely manner. These challenges are the focus of the modeling and parametric studies in this study in which, for the first time, a computational numerical model has been developed and validated for the tissue engineering of vascular grafts, based on fibrous scaffolds, and has been used for the optimization of these scaffolds.

Two types of mathematical approaches have been followed for the modeling of tissue engineering in scaffolds: (a) discrete cell dynamics models (Cheng, Youssef, Markenscoff, & Zygourakis, 2006; Engblom, Wilson, & Baker, 2018) and (b) continuum transport models for cells and nutrients (static conditions with only nutrient diffusion, chondrocytes: Chung, Yang, & Chen, 2006; Obradovic, Meldon, Freed, & Vunjak-Novakovic, 2000; Pisu, Lai, Cincotti, Concas, & Cao, 2004; dynamic conditions including flow and convection: Coletti, Maccietto, & Elvassore, 2006). Discrete dynamics simulations are typically associated with large computer memory requirements and long run times. Hence, the focus in this study is on a continuum transport model in a multiphase medium to represent a porous scaffold, with an additional growing cell phase and a permeating culture medium, where phase volume averaging has been applied (Gosman, Lekakou, Politis, Issa, & Looney, 1992; Lemon & King, 2007). The vast number of computational simulation studies in the literature, including recent ones, are dedicated to cartilage (Bandeiras & Completo, 2017; Y. Zhu et al., 2017) and bone tissue engineering (Bersini et al., 2016; Carlier et al., 2016; Guyot et al., 2014; Song et al., 2013; Song et al., 2015; Spencer, Hidalgo-Bastida, Cartmell, Halliday, & Care, 2013; Zhao, Vaughan, & Mcnamara, 2015). To the best of our knowledge, no such modeling and computational simulation studies have been published for vascular tissue engineering despite a plethora of experimental studies in the literature, and as such the present paper breaks new ground.

With regard to the tissue engineering of vascular grafts, an extensive literature search yielded that electrospun fiber scaffolds (Fu et al., 2014; He, Yong, Teo, Ma, & Ramakrishna, 2005; Mercado-Pagán, Kang, Findlay, & Yang, 2015; Nezarati, Eifert, Dempsey, & Cosgriff-Hernandez, 2015; G. C. Zhu et al., 2015) are most suitable for vascular grafts as they can be readily fabricated in the required tubular shape and any size of arteries, with controlled porosity and pore size and fiber orientation mimicking the orientation of collagen fibers in arteries (Elsayed, Lekakou, Labeed, & Tomlins, 2016a; Salifu, Nury, & Lekakou, 2011). Hence, the present study undertook the development of a continuum, two-phase model of the flow of culture medium and the transport of nutrients and cells through a fibrous scaffold, guided by the modeling of flow through fiber porous media for other applications, such as composites manufacturing (Amico & Lekakou, 2004; Lekakou, Edwards, Bell, & Amico, 2006).

Cell migration has been the focus of research within our group and we have identified directional differences in the 3D migration of cells, depending on the size and shape of cells in relation with the pores of the scaffold. In particular, such differences have been revealed in experimental tissue engineering studies between smooth muscle cells (SMCs; Elsayed, Lekakou, Labeed, & Tomlins, 2016b) and osteoblasts (Salifu, Lekakou, & Labeed, 2017) which points to the need for different phenomenological models of cell migration and proliferation for each type of cells with respect to the scaffold pore size and geometry. Therefore, a 3D cell migration model was adopted in our analysis for the SMC tissue engineering in fibrous scaffolds, with transverse and in-plane migration where different migration coefficients may be assigned in each direction. In this manner, the present study has seized the opportunity to elucidate the migration mechanism and directionality of SMCs in fibrous scaffolds, in the determination of the values of the migration coefficients in different directions through and across the fiber scaffold by fitting the model predictions to the experimental data of the SMC propagation.

In the current study, we have developed a transient, continuum, two-phase model of SMC tissue engineering in porous scaffolds for the fabrication of vascular grafts of tunica media. The model comprises transport equations for the flowing culture medium, the representative nutrient (oxygen) and the cells. A pioneering two-scale modeling approach has been adopted: the macroscale model includes transverse flow, nutrient diffusion, and cell migration through the scaffold continuum; a novel model has been developed at mesoscale, for the in-plane transport across a phenomenological pore in which cell proliferation is modeled following a layer-by-layer cell filling approach so that the pore size and properties are a function of time and the pore location in the scaffold. This innovative, comprehensive model was implemented in a computer code which will be validated in computer simulations of the SMC tissue engineering in an electrospun fiber scaffold under static and dynamic cell culture conditions, comparing the predictions with corresponding experimental data of previous experimental studies within our group. This will be followed by parametric studies to evaluate the impact of scaffold microstructure, cell dynamics, oxygen transport, and static or dynamic type of bioreactor on the rate and extent of cell proliferation. Furthermore, the scaffold microstructure will be optimized to tissue engineer a specified vascular graft within the shortest time whereas all parts of the graft maintain good access to oxygen dissolved in the culture medium, where oxygen is considered as a limiting factor for the growth and survival of SMCs.

2 | THEORETICAL MODELING

A transient, continuum two-phase model is proposed in this study with volume-averaged equations. The two phases comprise a solid phase, including the scaffold and attached cells, and a fluid phase including the culture medium with any dissolved oxygen and suspended cells. Figure 1 presents a conceptual microscale model at two different times to demonstrate different evolutionary processes in smooth muscle cell tissue engineering; the fibrous scaffold has an initial porosity and pore size distribution and the culture medium with suspended cells perfuses through the pores. Cells from the culture medium get attached to the surface of fibers, multiply and migrate in both the in-plane and transverse directions crawling on the surface of their substrate (fiber or cell underlayer), whereas the culture medium perfuses in 3D flow at the microscale. The attached cells connect into tissue, layer-by-layer inside each pore, reducing the pore size, and porosity as a function of time, until the whole pore has been filled and no more cell layers can be built up, allowing only cell migration. In this manner, the upstream pores in the perfusion macroflow direction are filled first where the pore filling in the model is envisaged to take place layer-by-layer in the *y*- direction (in-plane). Volume averaging is then applied to a volume unit, such as that presented in Figure 1, to derive the continuum flow, oxygen transport and cell transport equations of the theoretical model for the SMC tissue engineering through a porous scaffold.

Darcy's law (Brinkman, 1949) governs the perfusion flow of the culture medium through the porous scaffold with the mean flow being predominantly in the transverse, *x*-direction through the scaffold:

$$U = -\frac{\boldsymbol{k}}{\mu\varepsilon}\nabla P = -\frac{k_x}{\mu\varepsilon}\frac{\partial P}{\partial x} \tag{1}$$

where U is the mean velocity, P is the mean pressure, μ is the viscosity of the culture medium, ε is the porosity of the scaffold and k is the permeability tensor of the scaffold with k_x the permeability in the transverse direction. As the scaffold pores are filled with cells and the scaffold evolves from a fiber scaffold to a tissue graft, ε and k are dynamic properties, both generally reducing with time. The culture medium is considered as a Newtonian fluid.

For static conditions in a bioreactor with the scaffold placed under a static mass of culture medium with suspended cells and dissolved oxygen (Figure 2a), the pressure drop depends on the hydraulic head of the culture medium, H_1, above the scaffold top surface and the thickness of the scaffold, H:

$$\frac{\partial P}{\partial x} = \frac{\rho g H_1}{H} \tag{2}$$

where ρ is the density of the culture medium and g denotes the gravity: $9.81\,\mathrm{m\,s^{-2}}$. In the case of a bioreactor with the scaffold attached around a central, rotating shaft (Figure 2b), which rotates at a frequency, f (rotations per second), the pressure drop across the scaffold (or graft) thickness depends on the rotating speed and the shaft radius, R, according to the relation:

$$\frac{\partial P}{\partial x} = \rho 4\pi^2 f^2 (R_{\mathrm{shaft}} + H) \tag{3}$$

The oxygen transport across the scaffold is described using a perfusion–diffusion-reaction equation (Coletti et al., 2006; Nava, Raimondi, & Pietrabissa, 2013; Spencer et al., 2013) in two dimensions.

$$\frac{\partial C_{O_2}}{\partial t} + \frac{\partial U_{C_{O_2}}}{\partial x} = D_{O_2,x}\frac{\partial^2 C_{O_2}}{\partial x^2} + D_{O_2,y}\frac{\partial^2 C_{O_2}}{\partial y^2} - Q_{O_2} \tag{4}$$

where C_{O_2} is the oxygen concentration, t is the time, D_{O_2} is the diffusion coefficient of oxygen, and Q_{O_2} is the oxygen consumption rate. The oxygen transport equation includes the convection term due to perfusion in the *x*-direction through the depth of scaffold, oxygen diffusion in the transverse and in-plane directions, and oxygen consumption by the cells (the reaction term). An *x*-position in the scaffold is exposed to perfusion flow if the pore and pores in the upstream *x*-position are not filled; if the pores are blocked, locally $U = 0$. Oxygen diffusion in the *x*-direction occurs through the culture medium (treated as water), hence, $D_{O_2,x}$, was taken as the diffusion coefficient of oxygen in water (representing the culture medium). In the in-plane, *y*- direction from the center of the phenomenological pore to the fiber centreline, depending on the *y* position, oxygen diffusion occurs in the culture medium (D_{O_2} in water before the attached cell layer has been encountered), the cells (D_{O_2} in cells for the area fraction occupied by the cells at each position) and the solid scaffold (gelatin fibers in this study; D_{O_2} in gelatin for the area fraction occupied by the fiber scaffold at each position).

The reaction term of equation (4) representing oxygen consumption by the cells has been modeled by the following relation (Salifu, Elsayed, Lekakou, Labeed, & Tomlins, 2017):

$$Q_{O_2} = k_{O_2} C_{\mathrm{cell}} \tag{5}$$

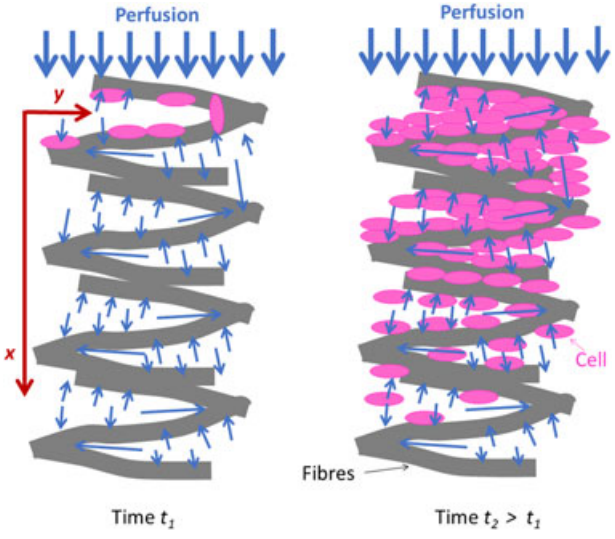

FIGURE 1 A conceptual microscale model for the perfusion of culture medium and 3D cell migration and proliferation in a fibrous scaffold; *x* is the transverse direction and y is an in-plane direction through the scaffold [Color figure can be viewed at wileyonlinelibrary.com]

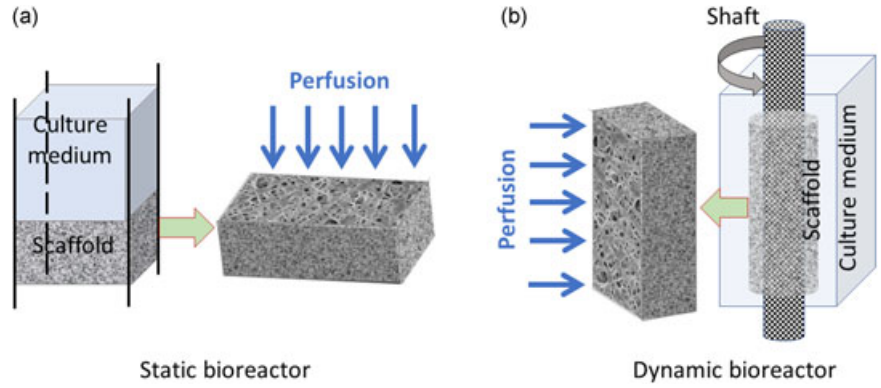

FIGURE 2 Diagram of the bioreactors simulated in the present numerical case-studies: (a) Bioreactor under static conditions. (b) Dynamic bioreactor with a rotating shaft and attached scaffold/graft (rotating with the shaft) [Color figure can be viewed at wileyonlinelibrary.com]

where the rate of oxygen consumption is proportional to the concentration of alive cells, C_{cell}, and k_{O_2} is a constant to be determined for each type of cells (Salifu, Elsayed et al., 2017).

The cellular dynamics is modeled using a transient equation where the cell concentration is a function of convection, cellular migration, growth, and death (Pohlmeyer, Waters, & Cummings, 2013; Spencer et al., 2013):

$$\frac{\partial C_{cell}}{\partial t} + \frac{\partial UC_{cell}}{\partial x} = \frac{D_x \partial^2 C_{cell}}{\partial x^2} + \frac{D_y \partial^2 C_{cell}}{\partial y^2} + Q_{cell\ growth} - Q_{cell\ death} \tag{6}$$

where D_x, D_y are the cell migration coefficients in the transverse x- and in-plane y- directions, respectively, $Q_{cell\ growth}$ is the cell growth rate, and $Q_{cell\ death}$ is the cell death rate. In the experiments simulated in the present study, the cells were seeded statically at the start of the tissue engineering process, in both the static and dynamic bioreactor environments, hence, no convection term was included in equation (6): $\frac{\partial UC_{cell}}{\partial x} = 0$.

Due to the relatively short period of tissue engineering monitoring in this study of 9 days, the term of cellular death was considered negligible:

$$Q_{cell\ death} = 0 \tag{7}$$

The growth rate of the cells is given by the relation (Salifu, Elsayed et al., 2017):

$$Q_{cell\ growth} = K_{growth} C_{cell} \tag{8}$$

where the Monod model has been used for the cell growth constant, K_{growth}, as a function of oxygen concentration and consumption, given by the following relation (Koch, 1998; Salifu, Elsayed et al., 2017):

$$K_{growth} = \frac{K_{growth,\,max}}{R_{O_{2,\,max}} - R_{O_{2,\,avg}}} \frac{dC_{oxygen}/dt}{C_{cell}} - R_{O_{2,\,avg}} \tag{9}$$

where $K_{growth,max}$ is the maximum smooth muscle cell growth rate, $R_{O_{2,max}}$ and $R_{O_{2,avg}}$ are the maximum and average oxygen consumption rate of cells, respectively. While the Monod equation does not include a term for the contact inhibition of cell growth, such as the Contois model (Contois, 1959) for example, in the model of the present study, the cell density is translated to a local area fraction of the scaffold covered by the cells at each (x, y) position, which depends on the cell density and the cell dimensions. When this local area fraction reaches 1 (full area coverage by the cells), one cell layer is completed at that location, and then a new, partially filled, cell layer is started. Hence, cell contact inhibition is taken into account in the present computational model.

As cells grow and proliferate they cover the surface of the fibers and fill the pore spaces in the scaffold. To mathematically demonstrate the decrease in porosity, it was considered that the solid fiber diameter increases as cells adhere to the fibers layer-by-layer. By inputting the average cell thickness and the number of cell layers locally adhering to the fibers, the new fiber diameter can be calculated. The porosity is then updated in terms of the ratio between the initial (d_o) and final (d) fiber diameters:

$$\varepsilon = \frac{\varepsilon_0 d_0^2}{d^2} \tag{10}$$

The value of the transverse permeability of the solid porous scaffold (including fibers and attached cells) is then updated using the Carman–Kozeny equation (Amico & Lekakou, 2004; Carman, 1937; Lekakou et al., 2006) using the updated values of porosity and fiber diameter.

$$k_x = k_{x,0}\left[\frac{d^2\varepsilon^3/(1-\varepsilon)^2}{d_0^3\varepsilon_0^3/(1-\varepsilon_0)^2}\right] \tag{11}$$

where ε is the updated porosity, ε_0 is the initial porosity and $k_{x,0}$ is the initial transverse permeability of the scaffold.

The equations were discretised using a time implicit, finite volume/finite difference numerical technique (Gosman et al., 1992). The 2D system of algebraic equations was solved in a two-substep numerical sweep for the two (x-, y-) directions (each time step divided into two-time substeps; Lekakou & Richardson, 1986), using the Thomas algorithm for solving the tridiagonal system of equations in each sweep. In the numerical discretization, the x and y continuous variables are translated into the i and j discrete variables, respectively. The phenomenological model of this study considers j to vary from 1 in the middle of a phenomenological pore in Figure 1 to j_{tot} in the middle of

the fiber. In the computational simulations, it was taken that the average cell thickness is an N multiple of Δy, with $N = 1$ in most simulations. In this manner, the filling of each cell layer at each j (and for each i position) can be monitored in the computer code, and the build-up of cell tissue, layer-by-layer can be computed from one j to j + 1 (at the same i, and for each i). The numerical model was implemented into a computer algorithm and Figure 3 presents the flowchart of this algorithm, illustrating the sequence of the numerical steps in this study, including the interactions between different processes and phenomena described by the corresponding equations.

3 | NUMERICAL CASE STUDIES

The numerical case-studies consider two types of bioreactor, as shown in Figure 2. A static bioreactor in which the culture medium is static (unstirred) above the scaffold and perfusion occurs through the scaffold under gravity. A dynamic bioreactor comprises a shaft with attached scaffold/graft around it, where the shaft rotates in the culture medium; in this case, the culture medium perfuses into the scaffold/graft under the action of pressure gradient generated by the circulating flow.

Table 1 presents the value of the input parameters used for the computational simulations to simulate experiments presented by Elsayed et al. (2016a, 2016b). In the experiments, gelatin fiber scaffolds were electrospun as stacks of alternating +45 and −45° unidirectional fiber layers, forming a bidirectional fiber assembly to optimize the mechanical properties of the scaffold (Elsayed et al., 2016a). The scaffold gelatin fibers were, subsequently, crosslinked using glutaraldehyde, as is described by Elsayed et al. (2016a). Two different crosslinked electrospun scaffolds, S1 and S2, were selected for further tissue engineering studies, where scaffold S1 is of lower porosity and smaller pore size and fiber diameter than S2, as is also summarized in Table 1. These scaffolds were seeded with human umbilical vein smooth muscle cells (SMCs) on their top surface, under static conditions according to the procedures described by Elsayed et al. (2016a). Tissue engineering experiments under static conditions were carried out by (Elsayed et al., 2016a, 2016b) and simulated in the present study to validate the models. All initial scaffold microstructural parameters used as input data in the model and presented in Table 1 refer to the measured mean values across the scaffold (mean fiber diameter, mean pore diameter, mean porosity; Elsayed et al., 2016a). The permeability measurements for these scaffolds and other electrospun scaffolds of different porosity, pore and fiber size (Elsayed et al., 2016a) were found to follow the Carman–Kozeny equation (Carman, 1937

$$k_x = \frac{1}{K}\frac{d^2\varepsilon^3}{(1-\varepsilon)^2} \tag{12}$$

with a Kozeny constant, $K = 0.032$ (Elsayed et al., 2016a). Although the Carman–Kozeny equation has been derived for viscous flow through tubular porous paths and was intended for flow through granular beds, over the years its applicability has been well proven for flows through fiber media (Amico & Lekakou, 2004), which is, in fact, the case for the scaffolds of this study. Following the initial simulations to validate the predictions against the corresponding experimental data for scaffolds S1 and S2 (Elsayed et al., 2016a, 2016b), parametric studies for different scaffolds of different porosity or other microstructural parameters were conducted for which the scaffold permeability was calculated using equation (12).

The case-study with the dynamic bioreactor (Figure 2b) involved an initial phase of cell seeding on the outer scaffold surface under static conditions, followed by the shaft rotation at a frequency, $f = 60$ rpm (Elsayed et al., 2016b).

In the SMC tissue engineering experiments described by Elsayed et al. (2016a, 2016b), samples of the cell-seeded scaffolds were removed after a certain number of days in the culture medium under static or dynamic conditions and subjected to a number of tests. For scanning electron microscopy (SEM), the samples were washed in phosphate buffered saline solution (phosphate buffered saline solution), fixed in 10 wt% glutaraldehyde overnight, dehydrated in a graded series of ethanol/water solution and dried in a vacuum desiccator overnight. After been sputter coated with 20 nm of 60:40 gold/palladium mix at 25 mA dc in a EEMS 575X sputter coater, they were examined using a Hitachi S3200 SEM at 15 kV. SEM images of each surface of the scaffold were analyzed to calculate the area

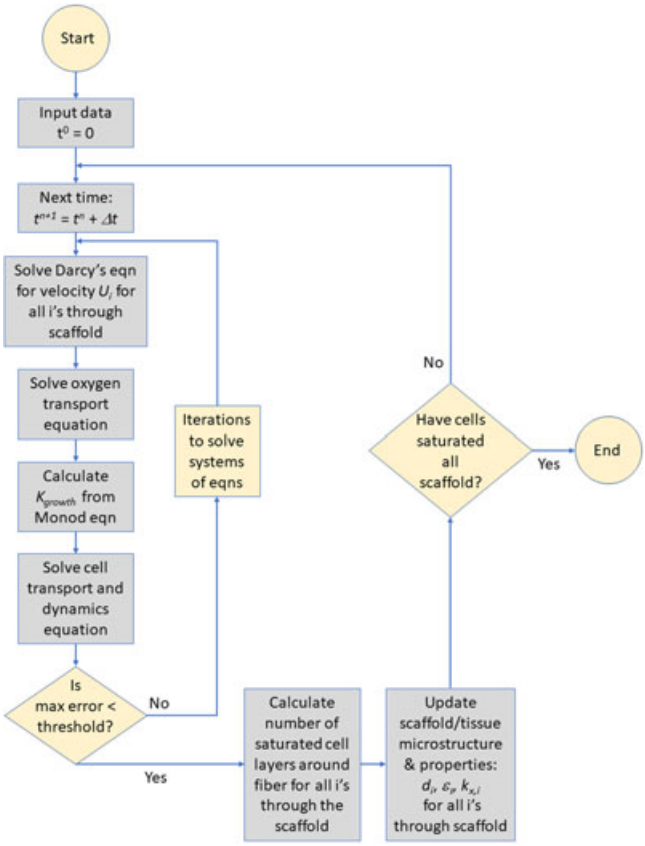

FIGURE 3 Flowchart of the computational algorithm for the numerical solution of the equations of the model presented in this study [Color figure can be viewed at wileyonlinelibrary.com]

TABLE 1 List of input parameters for the computational simulations

Scaffold	
Length, L (mm)	15
Width, W (mm)	15
Thickness, H (mm)	0.325
Swell ratio from dry to wet (immersed in water)	1.2 (Elsayed, 2013)
Scaffold S1	
Dry porosity, ε_0	0.74
Mean dry pore diameter (μm)	7
Mean dry fiber diameter, d_0 (μm)	1.78
Permeability, $k_{x,0}$ (m^2)	10^{-12}
Scaffold S2	
Dry porosity, ε_0	0.83
Mean dry pore diameter (μm)	16.2
Mean dry fiber diameter, d_0 (μm)	2.47
Permeability, $k_{x,0}$ (m^2)	7×10^{-12}
Culture medium	
Viscosity, μ (mPa·s)	1
Oxygen transport	
Initial oxygen concentration in culture medium-saturated (mol m^{-3})	0.284
Initial oxygen concentration in gelatin fibers-saturated (mol m^{-3})	0.04
Diffusion coefficient of O_2 in culture medium (water) (m^2 s^{-1})	2×10^{-9} (Elsayed et al., 2014
Diffusion coefficient of O_2 in gelatin fibers (m^2 s^{-1})	1.65×10^{-13} (Elsayed et al., 2014)
Diffusion coefficient of O_2 across cells (m^2 s^{-1})	2×10^{-9}
Oxygen consumption constant by SMCs, k_{O_2} (mol $cell^{-1}$ s^{-1})	9×10^{-16} (Salifu, Elsayed, et al., 2017)
SMC cellular kinetics	
Initial cell concentration in the culture medium (cells m^{-3})	2.5×10^{10} (Elsayed et al., 2016a, 2016b).
Initial area fraction of scaffold outer surface with seeded cells	0.4 (Elsayed et al., 2016a, 2016b).
Cell attachment constant (% of SMCs in the adjacent culture medium that adhere to scaffold)	35 (Elsayed et al., 2016a, 2016b)
Transverse cell migration coefficient, D_x (m^2 s^{-1})	8×10^{-28} static conditions320×10^{-28} dynamic conditions
In-plane cell migration coefficient, D_y (m^2 s^{-1})	0.8×10^{-28}
Average SMC cell thickness (μm)	1.45 (Elsayed et al, 2016a)).
Average SMC cell area (μm^2)	1200 (Elsayed et al. 2016a, 2016b)
Maximum SMC cell growth constant, $K_{growth,max}$ (s^{-1})	2.5×10^{-5} (Salifu, Elsayed, et al., 2017)
Average O_2 consumption rate by SMCs, $R_{O_2,avg}$ (s^{-1})	1.12×10^{-18} (Salifu, Elsayed, et al., 2017)

Note. SMC: smooth muscle cells.

fraction covered by cells (compared to the area fraction containing only fibers and pores without any cells). The SEM images and data are compared with the predictions of this study, where appropriate.

4 | RESULTS

Computational simulations of smooth muscle arterial tissue engineering were conducted for both a static and a dynamic bioreactor. In each case-study, a first set of simulations were conducted with the aim at validating the theoretical model and fitting the values for the cell migration coefficients, D_x, D_y, by comparing the predictions against experimental data (Elsayed et al., 2016a, 2016b). The second stage of computational simulations aimed at the optimization of the microstructural parameters of the scaffold, by conducting a series of parametric studies with different values of the scaffold porosity and fiber diameter and constructing maps from which the best parameters for a scaffold would be selected on the basis of maximum cell proliferation within the shortest time, whereas the predicted oxygen concentration is above the threshold that maintains cell survival.

4.1 | Static bioreactor

Figure 4 presents 3D maps of the cell area fraction as a function of distance from the seeded scaffold surface (also in direct contact with the culture medium) and the distance (j position) from the center of a phenomenological pore to the fiber surface. Scaffold S1 has a small average pore size of approximately 5.2 μm after being swollen with the culture medium, allowing for a maximum of two SMC cell layers across from the pore center to the fiber surface. The small pore size allows for very fast filling of the pores by the cells as is evident by the quick completion of the two cell layers at j = 1 and 2 in Figure 4a. The maximum depth of cell migration from the scaffold's seeded surface is around 120 μm after 3 days, 160 μm after 6 days, and 200 μm after 9 days. If taking the median normalized cell density of 0.5 as a reference point for a sufficiently filled layer to represent the propagating cell front, the distances traveled by the cells are around 85, 130, and 165 μm after 3, 6, and 9 days, respectively. Scaffold S2 has a much larger wet pore size which allows for more SMC cell layers. This results in a wider cell area fraction distribution amongst the j positions in the phenomenological pore, where after 9 days of cell culture, cells do not fill the core of the pore. The comparative

predictions for both scaffolds agree with the corresponding SEM images of the top surface of scaffold (seeded surface, in contact with the culture medium) also presented in Figure 4.

Two types of experimental data were used for the validation of the computational model. The first set of experimental data (Elsayed et al., 2016a, 2016b; Elsayed, 2013) comprise the depth covered by cells from the top (seeded) surface of the scaffold in time steps of three days: Measurements were conducted from SEM images and optical micrographs of sections stained with eosin solution for histomorphology (Elsayed et al., 2016a, 2016b; Elsayed, 2013; Lamprou, Zhdan, Labeed, & Lekakou, 2011). The experimental methodology utilized 10 measurements across the scaffold depth in each section, coupled with the use of at least three sections along its width to give a total of $n = 30$. The predicted cell front propagation through the depth of the scaffold was based on the definition of the cell front at a normalized cell density (cell area fraction) of 0.5 for the cell layer attached to the fiber surface. Figure 5a,b, demonstrate good agreement between the predictions of this study and the experimental data by Elsayed et al. (2016b), with the line of best fit through the predicted values after 3, 6, and 9 days of cell culture passing through the origin and crossing the experimental data for both scaffolds. Using these sets of experimental data, the cell migration coefficient in the transverse (*x*-) and in-plane (*y*-) directions was fitted to the values presented in Table 1 for a static bioreactor, and as can be seen, it was found that the migration coefficient of the SMCs is 10 times higher in the transverse direction through the fibrous scaffold than in the in-plane direction; these values were used for all scaffolds in the validation and parametric studies in a static bioreactor in section 4.1.

The second set of experimental data comprises 3-(4,5-dimethylthiazol-2-yl)-5-(3-carboxymethoxyphenyl)-2-(4-sulfophenyl)-2H-tetrazolium (MTS) assay absorbance measurements of light at 490 nm, representing cell proliferation across the entire scaffold (Elsayed et al., 2016b). Figure 5c demonstrates very good agreement between predictions and experimental data for Scaffold S1 for 3, 6, and 9 days in culture. Figure 5d shows very good agreement between the predictions and experiment for Days 3 and 9 but displays a higher predicted total cell number than the MTS acquired value on Day 6. One possible explanation could be that the dye used in the MTS assay was not able to diffuse properly in the samples and thus did not properly react with the growing cells, which would explain the lower return value measured on Day 6 for Scaffold S2. Differences between the mathematical model and the experimental scaffold also include nonuniform seeding of the scaffolds. It is, however, safe to assume a good validity for the mathematical model for all days of the cell culture before cell apoptosis, making the mathematical model and corresponding computer code a suitable tool to be used in the optimization of the scaffold for the tissue engineering processes.

As cells grow, their environment changes: the scaffold porosity decreases as more pore fraction is taken up by the cells, scaffold

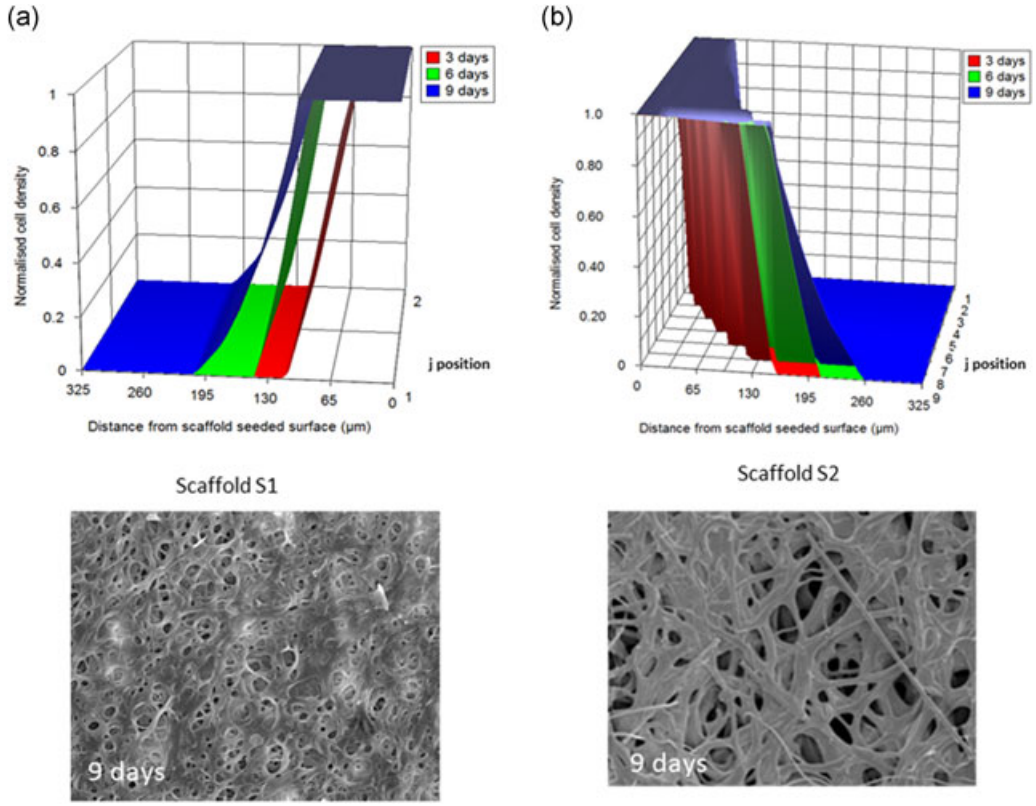

FIGURE 4 3D map of predicted normalized cell density (area fraction) across (a) Scaffold S1 and (b) Scaffold S2 for 3 (red), 6 (green), and 9 (blue) days of static cell culture. SEM micrographs of the top surface (in contact with culture medium) of each scaffold after 9 days of static cell culture (Elsayed, 2013). SEM: scanning electron microscope [Color figure can be viewed at wileyonlinelibrary.com]

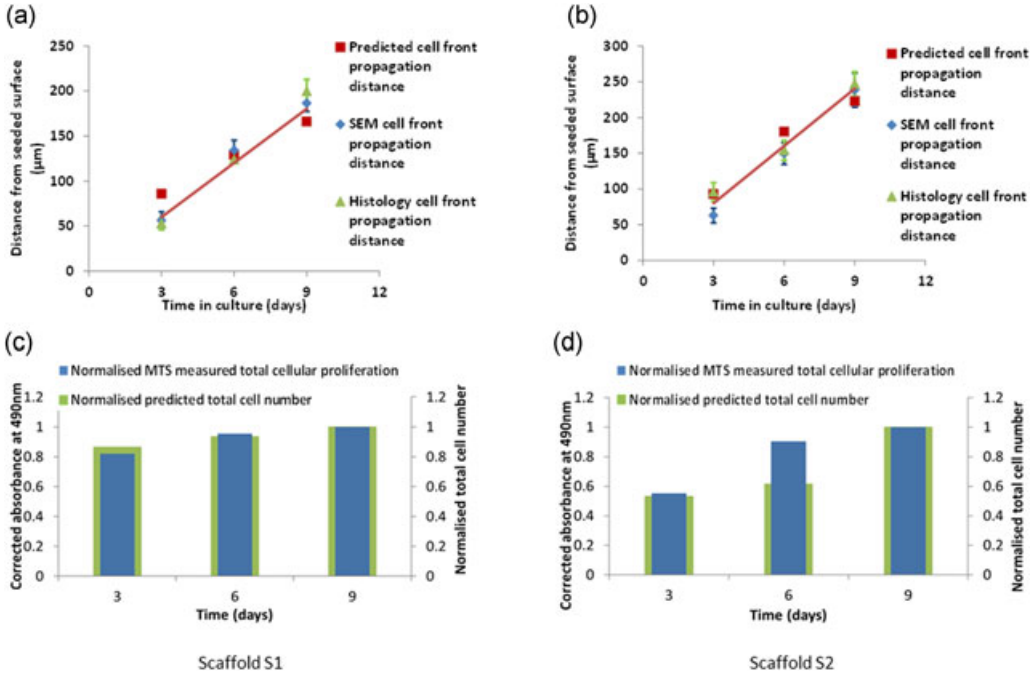

FIGURE 5 Comparison of the model predictions against experimental data (Elsayed et al, 2016b; Elsayed, 2013) of progress of the cell front through the depth of scaffold from SEM images or histology of stained sections (a,b) and the MTS assay data of cell proliferation (c,d) across the whole scaffold after 3, 6 and 9 days of static cell culture for scaffolds S1 (a,c) and S2 (b,d). MTS: 3-(4,5-dimethylthiazol-2-yl)-5-(3-carboxymethoxyphenyl)-2-(4-sulfophenyl)-2H-tetrazolium; SEM: scanning electron microscope

permeability to the perfusion of the culture medium drops and the cells populating the scaffold consume the available oxygen at higher rates. Figure 6 shows the predicted oxygen concentration profiles across the depth of the scaffolds as the environment changes over the 9 days of cell culture. It is evident that oxygen concentration falls faster and to lower values for Scaffold S1, which has smaller pores and lower porosity than Scaffold S2.

In the second stage of computational simulations for a static bioreactor, the validated numerical model and computer code was used in parametric SMC tissue engineering studies for scaffolds with a range of fiber diameters and porosities. Taking into account the range of such fiber structures that can be electrospun, the SMC cell dimensions and the requirement for a certain level of required tensile strength for scaffolds to be used in SMC tissue engineering for use as vascular tunica media replacement (to be discussed in more detail in following section 5) as well as the mechanical characterization of the electrospun scaffolds considered in this study and reported in (Elsayed et al., 2016a), the set of presented parametric studies includes scaffolds with porosities of 72–80% and fiber diameters of 2–5 μm. Figure 7a,b present contour plots of the predicted total cellular proliferation, as a total cell number across the entire scaffold, and the predicted cell front propagation distance from the seeded surface of the scaffold, respectively, after 9 days in culture for all simulated scaffolds. There seems to be a direct relationship of scaffold porosity and fiber diameter with the cellular proliferation, where scaffolds of higher porosity and larger fiber diameter support more cells and the cell front has propagated deeper in the scaffolds after 9 days in culture. Figure 7c presents contour plots of the

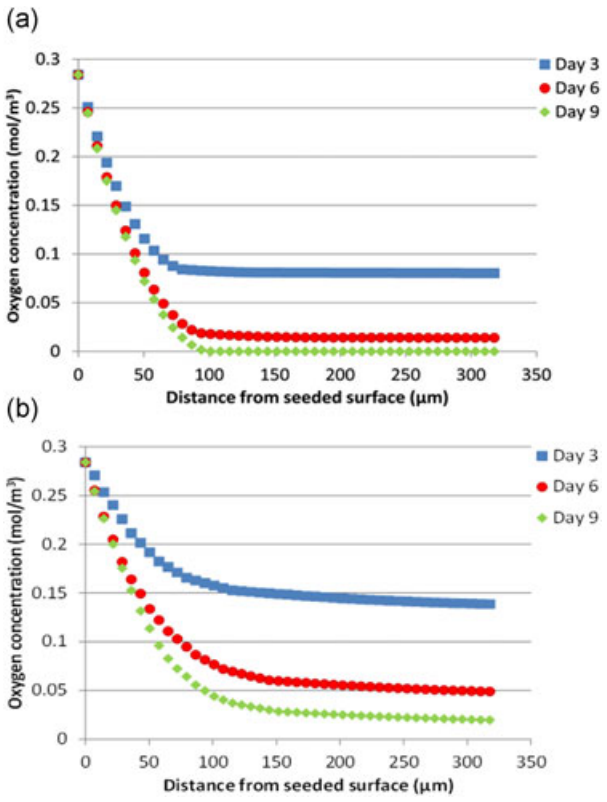

FIGURE 6 Predicted oxygen concentration profiles at the center of the phenomenological pore (at j = 1, pore may be unfilled or filled with cell layers) after 3 (blue), 6 (green), and 9 (red) days of static cell culture: (a) Scaffold S1, (b) Scaffold S2 [Color figure can be viewed at wileyonlinelibrary.com]

maximum distance from the surface of the scaffold that maintains the minimum oxygen concentration (0.028 mol/m^3) after 9 days of culture; The three contour plots in Figure 7a,b, and c seem all directly correlated.

Assuming symmetry, if a scaffold is seeded from both sides, a scaffold of 0.4 mm thickness can be cultured in-vitro under static conditions and be fully populated after 9 days of culture; the main drawback of such a system is the fact that after 9 days, cells over 100 μm distance from the surface would have difficulty surviving due to the reduced oxygen concentration. One solution is to grow the scaffolds for only 6 days of culture in-vitro before being transplanted. Figure 7d,e,f show contour plots of the predicted cellular proliferation, cell front propagation distance and the distance from the surface that maintains the minimum required oxygen concentration after 6 days of static cell culture.

4.2 | Dynamic bioreactor

Scaffold S2 was selected for the model validation under dynamic tissue engineering conditions, as it showed the highest level of cellular proliferation in the static bioreactor. Predictions of the local alive cell area fraction from the computer simulations were compared to data from SEM images of the outer (cell seeded) and inner (unseeded) surfaces of the seeded scaffold after 3 and 6 days in the dynamic bioreactor (Figure 2b; Elsayed, 2013) to adjust the cell migration coefficient under dynamic conditions. Figure 8 demonstrates good agreement between experimental data and predictions which was achieved by fitting the cell transverse migration coefficient to $D_x = 320 \times 10^{-28}$ m^2·s^{-1}, 40 times higher than in the static bioreactor, to take into account the enhancement of cell migration under dynamic conditions due to the increased shear forces of Darcy's flow through the scaffold and the centripetal forces. This value of D_x was then used in all parametric study simulations in the dynamic bioreactor. In any case, both predictions and experimental data in Figure 8 demonstrate that cell proliferation has progressed across the whole thickness of 325 μm of scaffold S2 after 6 days in culture in the dynamic bioreactor compared to half such progress in the static bioreactor in Figure 5b. Furthermore, the predicted oxygen profiles presented in Figure 8 show that oxygen concentration is maintained above the threshold limit of 0.028 mol/m^3 throughout the whole scaffold S2 for all 6 days of culture.

Using the validated computational model and code under dynamic conditions, further computer simulations were conducted for additional parametric studies for scaffolds of 3.5 μm fiber diameter and porosity in the range of 72–80%, seeded on one side (outer side) and placed in the dynamic bioreactor of Figure 2b, wrapping the rotating shaft. Figure 9 presents contour plots of the predictions of the total number of cells, the progress of the cell front from the seeded surface, and the depth of minimum oxygen concentration (0.028 mol/m^3) after 2, 3, and 6 days in the dynamic bioreactor. It can be seen that large fiber diameter and high porosity of scaffold favors total cell proliferation whereas high porosity favors oxygen penetration. However, large fiber diameter favors cell migration and proliferation through the scaffold thickness, which reaches a maximum propagation depth of 400 μm from the cell seeded surface for a scaffold porosity of 75% (dry) after 2 days of culture in the dynamic bioreactor.

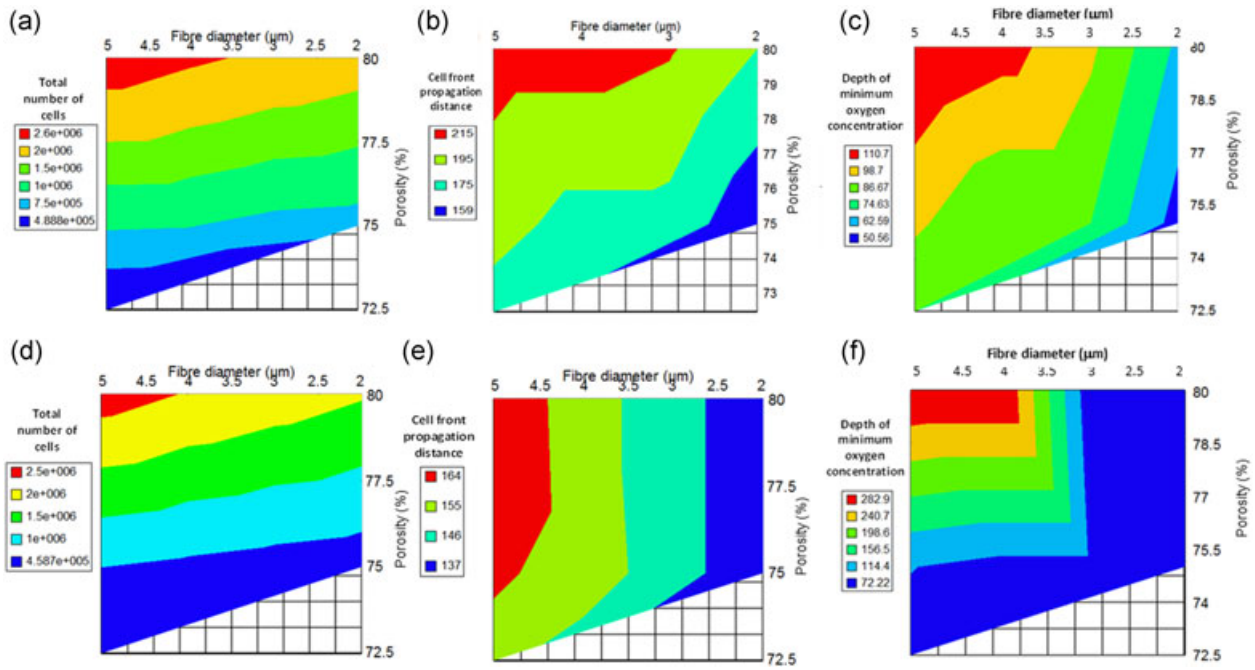

FIGURE 7 Contour plots of the predicted total cellular proliferation, cell front propagation distance (μm) from the seeded surface of the scaffold, and maximum distance (μm) from the seeded surface of the scaffold that maintains the minimum oxygen concentration (0.028 mol/m^3); (a,b,c) after 9 days of culture and (d,e,f) after 6 days of static cell culture [Color figure can be viewed at wileyonlinelibrary.com]

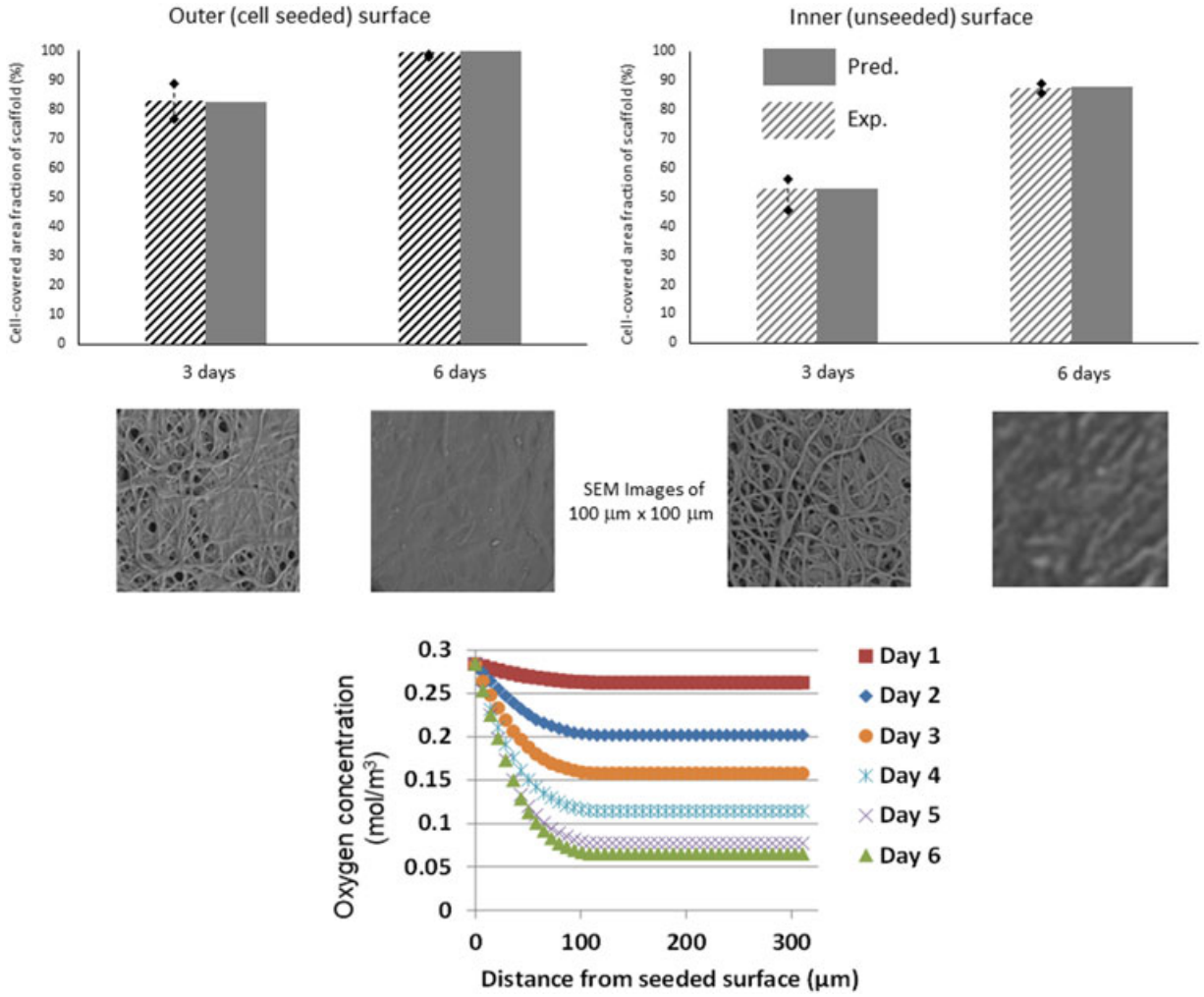

FIGURE 8 Computer simulation predictions of cell proliferation at the outer (cell seeded) and inner (unseeded) surface of Scaffold S2 (and comparison with experimental data and SEM images of the corresponding scaffold/graft surfaces from the experimental study; Elsayed, 2013) and predicted oxygen concentration profiles through the scaffold as a function of culture time in the dynamic bioreactor. SEM: scanning electron microscope [Color figure can be viewed at wileyonlinelibrary.com]

5 | DISCUSSION

All presented case studies considered a scaffold thickness equivalent to that of the tunica media of arteries, where this is 0.32 ± 0.1 mm for the left anterior descending (LAD) coronary artery (Holzapfel, 2005; Gradus-Pizlo et al., 2003) out of a total wall thickness of 0.7–0.9 mm for the coronary artery (Waller et al., 1992). The saphenous vein, often used as a graft for the coronary artery, has a total wall thickness of 0.400 ± 0.120 mm for thin-walled veins to 0.565 ± 0.138 mm for thick-walled veins (Human, Franz, Scherman, Moodley, & Zilla, 2009). Hence, the aim has been to engineer an SMC-filled tunica media graft of a thickness of 0.300–0.400 mm, within a reasonable time of a few days maximum, with all SMC layers having access to nutrients (represented by dissolved oxygen in this study, as the critical nutrient for SMCs), and the mechanical properties of the graft being equivalent to those of the natural arteries. Given that Young's modulus, E, and tensile strength, σ_F, of the tunica media and adventitia layers of the coronary artery in the circumferential and axial direction are (Waller et al., 1992): $E_{adventitia,circ} = 2.2$ MPa, $E_{adventitia,axial} = 1.5$ MPa, $E_{media,circ} = 0.55$ MPa, $E_{media,axial} = 0.57$ MPa, $\sigma_{F,adventitia,circ} = 1.4$ MPa, and $\sigma_{F,adventitia,axial} = 1.3$ MPa, $\sigma_{F,media,circ} = 0.45$ MPa and $\sigma_{F,media,axial} = 0.42$ MPa, a suitable range of scaffold porosity was selected for the vascular scaffolds to match the above properties. In earlier studies within our group (Elsayed et al., 2016a), it was found that acellular, crosslinked, electrospun, ±45° oriented gelatin fiber scaffolds reached Young's modulus of 0.4–1 MPa (for both circumferential and axial directions), a tensile strength of 0.6–1.5 MPa in the circumferential direction and 0.45–0.7 MPa in the axial direction, and a suture retention strength of 1.81–1.94 MPa, for dry porosity in the range of 75–62%, respectively (also compared to the suture retention strength of fresh saphenous vein of 1.81 MPa; Schaner et al., 2004). Hence, it has been thought that scaffolds of dry porosity in the range of 62–75% would match the mechanical properties of the tunica media of natural human arteries and the suture retention strength of the saphenous vein.

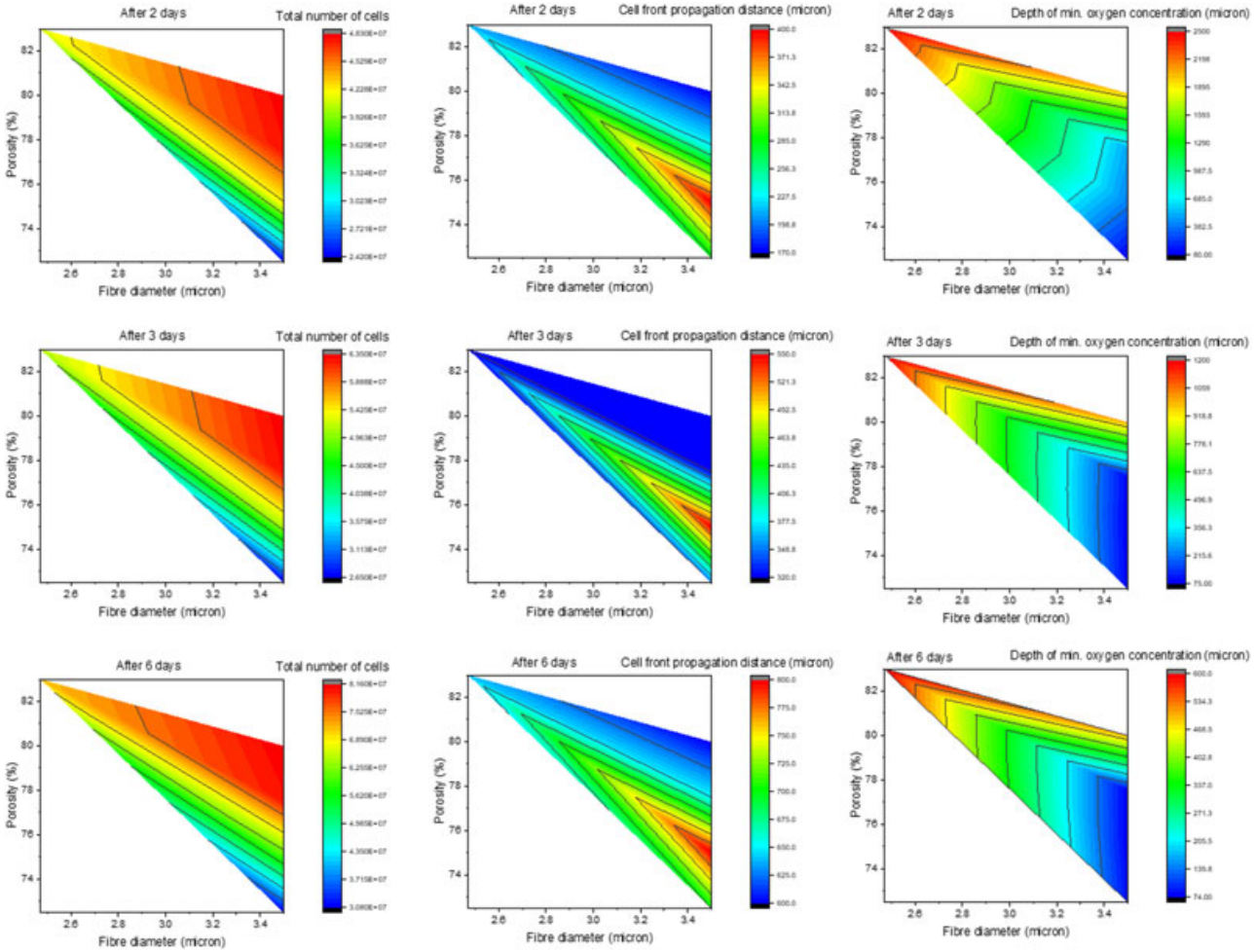

FIGURE 9 Contour plots of the predicted total cellular proliferation, cell front propagation distance (μm) from the seeded surface of the scaffold, and maximum distance (μm) from the seeded surface of the scaffold that maintains the minimum oxygen concentration (0.028 mol/m^3) after 2, 3, and 6 days of dynamic cell culture [Color figure can be viewed at wileyonlinelibrary.com]

The results of the parametric studies for SMC tissue engineering under static culture conditions in Figure 7 indicate that even after 9 days the cell front reaches only a distance of 0.215 mm for scaffolds of high dry porosity 79–80%, i.e., a tunica media graft of 0.3–0.4 mm cannot be tissue engineered within 9 days. This can be explained by the predicted progress of cell front in Figure 4, where it can be observed that after a fast rate of cellular proliferation and migration during the first 3 days, the rate of cell migration through the scaffold is subsequently reduced, due to the difficulty the cells have to migrate through smaller pores and cell-filled layers.

In the meanwhile, Figure 7c, indicates that the depth of minimum oxygen concentration is only 0.11 mm after 9 days for the high dry porosity scaffolds (79–80%) and becomes worse for scaffolds of dry porosity below 78%. Two factors come into play to determine oxygen concentration at any position within the scaffold: the first is the availability of a fresh supply of oxygen via convection in the perfusion of the culture medium from the surface, and the second is the density of the cells consuming the available dissolved oxygen. A large cell density means not only fast consumption of the existing oxygen but also filling of the pores and blocking them to the perfusion of culture medium to supply cells with more oxygen. The availability of oxygen deeper within the scaffold ensures not only the survival of existing cells but also increases cellular proliferation, followed by further migration. Consequently, a fall in the oxygen concentration below the threshold of 0.028 mol/m^3 is detrimental to cell proliferation and any progress of the cell front through the scaffold.

The case study of tissue engineering under dynamic culture conditions in a bioreactor with a rotating shaft on which the tubular scaffold is attached (Figure 2b) revealed (Figure 8) enhanced and much faster cell proliferation which is attributed to the additional forced permeation of culture medium, due to the pressure gradient generated by the circulating flow, and the 40-fold increase of the cell migration coefficient in the transverse direction through the scaffold for the same reason and the increased shear stresses that are generated. The predictions from parametric studies in Figure 9 demonstrate that the competing factors of fast initial cell migration and growth in scaffolds of high porosity and subsequent decline in the oxygen concentration and further cell growth, due to high local cell densities consuming oxygen and blocking pores, leading to an optimum scaffold dry

porosity of 75%: in such scaffolds the cell front can reach a depth of 0.4 mm from the cell-seeded surface after only 2 days in the dynamic bioreactor, whereas the scaffold at this depth still maintains an oxygen concentration above the threshold of 0.028 mol/m^3. This is most encouraging as a scaffold of 75% dry porosity has similar mechanical properties to those of the tunica media of the human coronary artery and the same suture retention strength as a human saphenous vein, frequently used as a vascular graft for the coronary artery, whereas such scaffold can be tissue engineered with SMCs within two days of dynamic culture.

The so tissue engineered tunica media graft could be inserted in an already electrospun fiber scaffold of larger diameter and the wall thickness of 0.5 mm to represent the adventitia layer of the LAD coronary artery in humans (Gradus-Pizlo et al., 2003). The adventitia graft scaffold should have very small fiber and pore diameter and low porosity to increase the mechanical properties of the vascular graft overall (Holzapfel, Sommer, Gasser, & Regitnig, 2005) and prevent any migration of SMCs from the tunica media graft layer whereas, on the other hand, allows the perfusion of oxygenated blood from capillaries and arterioles from the vasa vasorum through the adventitia and further to the tunica media graft, in vivo after implantation of the whole vascular graft, and acts as scaffold for angiogenesis in vivo.

6 | CONCLUSIONS

A transient, continuum, and the two-phase model of SMC tissue engineering with a novel model for local transport through a phenomenological pore in the scaffold, following a layer-by-layer cell filling approach, has been presented and validated successfully in this paper against corresponding experimental data of SMC proliferation in electrospun gelatin fiber scaffolds from previous studies within our group (Elsayerd et al., 2016a, 2016b). The fitting of the cell migration coefficients to match predictions with experimental data revealed that SMC migration takes place in both transverse and in-plane directions across the investigated fibrous scaffolds, with transverse SMC migration through the scaffold being dominant in both static and dynamic culture conditions. Furthermore, it was demonstrated that a dynamic bioreactor with a rotating shaft on which the tubular scaffold was attached leads to a 40-fold increase of the transverse cell migration coefficient and enhanced nutrient transport due to forced convection by the additional pressure drop of the circulating flow.

One of the most interesting aspects of the presented simulations and parametric studies is the conclusion that there are significant problems in trying to engineer replacement tissue in vitro in the absence of a viable blood network supply to the new tissue, where the predictions highlighted the fact that there are physical limitations to the number of cells that can be supported in a 3D scaffold due to the consumption of oxygen by the cells and the blocking of the pores to the perfusion of any culture medium supply, once the pores have been filled with cells.

However, despite such difficulties, systematic computer simulations and parametric studies of different types of scaffolds in the dynamic bioreactor revealed an optimized scaffold of 75% dry porosity that can be SMC tissue engineered into a viable graft of the tunica media of the coronary artery within 2 days in the dynamic bioreactor whereas oxygen concentration is still maintained above the threshold of 0.028 mol/m^3 (required for cell survival) throughout the whole graft. Such scaffold also matches the mechanical properties of the tunica media of the human coronary artery and the suture retention strength of a saphenous vein, often used as a graft for the coronary artery at present.

ACKNOWLEDGEMENTS

The authors gratefully acknowledge the funding of this project by the University of Surrey-NPL Partnership.

ORCID

Constantina Lekakou http://orcid.org/0000-0003-4494-1761

REFERENCES

Amico, S., & Lekakou, C. (2004). Flow through a two-scale porosity, oriented fibre porous medium. *Transport in Porous Media*, *54*, 35–53. https://doi.org/10.1023/A:1025799404038

Bandeiras, C., & Completo, A. (2017). A mathematical model of tissue-engineered cartilage development under cyclic compressive loading. *Biomechanics and Modelling in Mechanobiology*, *16*, 651–666. https://doi.org/10.1007/s10237-016-0843-9

Bersini, S., Gilardi, M., Arrigoni, C., Talò, G., Zamai, M., Zagra, L., … Moretti, M. (2016). Human in vitro 3D co-culture model to engineer vascularized bone-mimicking tissues combining computational tools and statistical experimental approach. *Biomaterials*, *76*, 157–172. https://doi.org/10.1016/j.biomaterials.2015.10.057

Brinkman, H. C. (1949). *A calculation of the viscous force exerted by a flowing fluid on a dense swarm of particles* (First.). The Netherlands: Springer.

Carlier, A., Skvortsov, G. A., Hafezi, F., Ferraris, E., Patterson, J., Koç, B., & Van Oosterwyck Oosterwyck, H. (2016). Computational model-informed design and bioprinting of cell patterned constructs for bone tissue engineering. *Biofabrication*, *8*, 025009. 17pp. https://doi.org/10.1088/1758-5090/8/2/025009/meta

Carman, P. C. (1937). Fluid flow through granular beds. *Transactions of the Institution of Chemical Engineers*, *15*, 150–S48. https://doi.org/10.1016/S0263-8762(97)80003-2

Chapman, S. K., Langley, J. A., Hart, S. C., & Koch, G. W. (1998). The Monod model and its alternatives. In A. L. Koch, J. A. Robinson, & G. A. Milliken (Eds.), *Mathematical Modeling in Microbial Ecology. Chapman & Hall Microbiology Series (Physiology/Ecology/Molecular Biology/Biotechnology)* (*169*, pp. 62–93). Boston, MA: Springer. https://doi.org/10.1007/978-1-4615-4078-6_4

Cheng, G., Youssef, B. B., Markenscoff, P., & Zygourakis, K. (2006). Cell population dynamics modulate the rates of tissue growth processes. *Biophysical Journal*, *90*, 713–724. https://doi.org/10.1529/biophysj.105.063701

Chung, C. A., Yang, C. W., & Chen, C. W. (2006). Analysis of cell growth and diffusion in a scaffold for cartilage tissue engineering. *Biotechnology and Bioengineering*, *94*, 1138–1146. https://doi.org/10.1002/bit.20944

Coletti, F., Maccietto, S., & Elvassore, N. (2006). Mathematical modeling of three-dimensional cell cultures in perfusion bioreactors. *Industrial & Engineering Chemistry Research*, *5*, 8158–8169. https://doi.org/10.1016/S1570-7946(06)80292-0

Contois, D. E. (1959). Kinetics of bacterial growth: Relationship between population density and specific growth rate of continuous cultures. *Journal of General Microbiology*, *21*, 40–50. https://doi.org/10.1099/00221287-21-1-40

Croll, T. I., Gentz, S., Mueller, K., Davidson, M., O'Connor, A. J., Stevens, G. W., & Cooper-White, J. J. (2005). Modeling oxygen diffusion and cell growth in a porous, vascularising scaffold for soft tissue engineering applications. *Chemical Engineering Science*, *60*, 4924–4934. https://doi.org/10.1016/j.ces.2005.03.051

Daly, A. C., Sathy, B. N., & Kelly, D. J. (2018). Engineering large cartilage tissues using dynamic bioreactor culture at defined oxygen conditions. *Journal of Tissue Engineering*, *9*, 1–12. https://doi.org/10.1177/2041731417753718

Dzobo, K., Thomford, N. E., Senthebane, D. A., Shipanga, H., Rowe, A., Dandara, C., … Motaung, K. S. C. M. (2018). Advances in regenerative medicine and tissue engineering: Innovation and transformation of medicine. *Stem Cells International*, *2018*, 2495848–24. 24 pp. https://doi.org/10.1155/2018/2495848

Elsayed , Y. (2013). Fabrication and characterisation of scaffolds for tissue engineered vascular grafts (PhD Thesis), Guildford, UK, University of Surrey.

Elsayed, Y., Lekakou, C., & Tomlins, P. (2014). Monitoring and modeling of oxygen transport through uncrosslinked and crosslinked gelatin gels. *Polymer Testing*, *40*, 106–115. https://doi.org/10.1016/j.polymertesting.2014.08.016

Elsayed, Y., Lekakou, C., Labeed, F., & Tomlins, P. (2016a). Fabrication and characterisation of biomimetic, electrospun gelatin fibre scaffolds for tunica media-equivalent, tissue engineered vascular grafts. *Materials Science & Engineering C*, *61*, 473–483. https://doi.org/10.1016/j.msec.2015.12.081

Elsayed, Y., Lekakou, C., Labeed, F., & Tomlins, P. (2016b). Smooth muscle tissue engineering in crosslinked electrospun gelatin scaffolds. *Journal of Biomedical Materials Research*, *104*, 313–321. https://doi.org/10.1002/jbm.a.35565

Engblom, S., Wilson, D. B., & Baker, R. E. (2018). Scalable population-level modelling of biological cells incorporating mechanics and kinetics in continuous time. *Royal Society Open Science*, *5*, 180379. 7pp. https://doi.org/10.1098/rsos.180379

Fu, W., Liu, Z., Feng, B., Hu, R., He, X., Wang, H., … Wang, W. (2014). Electrospun gelatin/PCLand collagen/PLCLscaffolds for vascular tissue engineering. *International Journal of Nanomedicine*, *9*, 2335–2344. https://doi.org/10.2147/IJN.S61375

Gosman, A. D., Lekakou, C., Politis, S., Issa, R. I., & Looney, M. K. (1992). Multidimensional modeling of turbulent two-phase flows in stirred vessels. *AIChE Journal*, *38*, 1946–1956. https://doi.org/10.1002/aic.690381210

Gradus-Pizlo, I., Bigelow, B., Mahomed, Y., Sawada, S. G., Rieger, K., & Feigenbaum, H. (2003). Left anterior descending coronary artery wall thickness measured by high-frequency transthoracic and epicardial echocardiography includes adventitia. *The American Journal of Cardiology*, *91*, 27–32. https://doi.org/10.1016/S0002-9149(02)02993-4

Guyot, Y., Papantoniou, I., Chai, Y. C., Van Bael Bael, S., Schrooten, J., & Geris, L. (2014). A computational model for cell/ECM growth on 3D surfaces using the level set method: A bone tissue engineering case study. *Biomechanics and Modeling in Mechanobiology*, *13*, 1361–1371. https://doi.org/10.1007/s10237-014-0577-5

He, W., Yong, T., Teo, W. E., Ma, Z., & Ramakrishna, S. (2005). Fabrication and endothelialization of collagen-blended biodegradable polymer nanofibers: Potential vascular graft for blood vessel tissue engineering. *Tissue Engineering*, *11*, 1574–1588. https://doi.org/10.1089/ten.2005.11.1574

Holzapfel, G. A., Sommer, G., Gasser, C. T., & Regitnig, P. (2005). Determination of layer-specific mechanical properties of human coronary arteries with nonatherosclerotic intimal thickening and related constitutive modeling. *American Journal of Physiology: Heart and Circulatory Physiology*, *289*, 2048–2058. https://doi.org/10.1152/ajpheart.00934.2004

Human, P., Franz, T., Scherman, J., Moodley, L., & Zilla, P. (2009). Dimensional analysis of human saphenous vein grafts: Implications for external mesh support. *The Journal of Thoracic and Cardiovascular Surgery*, *137*, 1101–1108. https://doi.org/10.1016/j.jtcvs.2008.10.040

Lamprou, D., Zhdan, P., Labeed, F., & Lekakou, C. (2011). Gelatine and gelatine/elastin nanocomposites for vascular grafts: Processing and characterisation. *Journal of Biomaterials Applications*, *26*, 209–226. https://doi.org/10.1177/0885328210364429

Lekakou, C., Edwards, S., Bell, G., & Amico, S. C. (2006). Computer modelling for the prediction of the in-plane permeability of non-crimp stitch bonded fabrics. *Composites A: Applied Science and Manufacturing*, *37*, 820–825. https://doi.org/10.1016/j.compositesa.2005.04.002

Lekakou, C. N., & Richardson, S. M. (1986). Simulation of reacting flow during filling in reaction injection moulding (RIM). *Polymer Engineering Science*, *26*, 1264–1275. https://doi.org/10.1002/pen.760261806

Lemon, G., & King, J. R. (2007). Multiphase modeling of cell behavior on artificial scaffolds: Effects of nutrient depletion and spatially nonuniform porosity. *Mathematical Medicine and Biology*, *24*, 57–83. https://doi.org/10.1093/imammb/dql020

Mercado-Pagán, Á. E., Kang, Y., Findlay, M. W., & Yang, Y. (2015). Development and evaluation of elastomeric hollow fiber membranes as small diameter vascular graft substitutes. *Materials Science & Engineering*, *49*, 541–548. https://doi.org/10.1016/j.msec.2015.01.051

Nava, M. M., Raimondi, M. T., & Pietrabissa, R. (2013). A multiphysics 3D model of tissue growth under interstitial perfusion in a tissue-engineering bioreactor. *Biomechanics and Modeling in Mechanobiology*, *12*, 1169–1179. https://doi.org/10.1007/s10237-013-0473-4

Nezarati, R. M., Eifert, M. B., Dempsey, D. K., & Cosgriff-Hernandez, E. (2015). Electrospun vascular grafts with improved compliance matching to native vessels. *Journal of Biomedical Materials Research*, *103*, 313–323. https://doi.org/10.1002/jbm.b.33201

Nguyen, B.-N. B., Ko, H., Moriarty, R. A., Etheridge, J. M., & Fisher, J. P. (2016). Dynamic bioreactor culture of high volume engineered bone tissue. *Tissue Engineering*, *22*(3-4), 263–271. https://doi.org/10.1089/ten.tea.2015.0395

Obradovic, B., Meldon, J. H., Freed, L. E., & Vunjak-Novakovic, G. (2000). Glycosaminoglycan deposition in engineered cartilage: Experiments and mathematical model. *AIChE Journal*, *46*, 1860–1871. https://doi.org/pdf/10.1002/aic.690460914

Pierre, J., Gemmiti, C. V., Kolambkar, Y. M., Oddou, C., & Guldberg, R. E. (2008). Theoretical analysis of engineered cartilage oxygenation: Influence of construct thickness and media flow rate. *Biomechanics and Modeling in Mechanobiology*, *7*, 497–510. https://doi.org/10.1007/s10237-007-0107-9

Pisu, M., Lai, N., Cincotti, A., Concas, A., & Cao, G. (2004). Modeling of engineered cartilage growth in rotating bioreactors. *Chemical Engineering Science*, *59*, 5035–5040. https://doi.org/10.1016/j.ces.2004.07.101

Pohlmeyer, J. V., Waters, S. L., & Cummings, L. J. (2013). Mathematical model of growth factor driven haptotaxis and proliferation in a tissue engineering scaffold. *Bulletin of Mathematical Biology*, *75*, 393–427. https://doi.org/10.1007/s11538-013-9810-0

Rouwkema, J., & Khademhosseini, A. (2016). Vascularization and angiogenesis in tissue engineering: Beyond creating static networks. *Trends in Biotechnology*, *34*, 733–745. https://doi.org/10.1016/j.tibtech.2016.03.002

Salifu, A., Elsayed, Y., Lekakou, C., Labeed, F., & Tomlins, P. (2017). Cell dynamics of smooth muscle cells and osteoblasts for tissue engineer-

ing applications. *Journal of Biomaterials and Tissue Engineering*, *7*, 504–510. https://doi.org/10.1166/jbt.2017.1595

Salifu, A. A., Nury, B. D., & Lekakou, C. (2011). Electrospinning of nanocomposite fibrillar tubular and flat scaffolds with controlled fiber orientation. *Annals of Biomedical Engineering*, *39*, 2510–2520. https://doi.org/10.1007/s10439-011-0350-1

Salifu, A. A., Lekakou, C., & Labeed, F. (2017). Multilayer cellular stacks of gelatin-hydroxyapatite fiber scaffolds for bone tissue engineering. *Journal of Biomedical Materials Research*, *105*, 779–789. https://doi.org/10.1002/jbm.a.35954

Schaner, P. J., Martin, N. D., Tulenko, T. N., Shapiro, I. M., Tarola, N. A., Leichter, R. F., … Dimuzio, P. J. (2004). Decellularized vein as a potential scaffold for vascular tissue engineering. *Journal of Vascular Surgery*, *40*, 146–153. https://doi.org/10.1016/j.jvs.2004.03.033

Sengers, B. G., Van Donkelaar Donkelaar, C. C., Oomens, C. W. J., & Baaijens, F. P. T. (2005). Computational study of culture conditions and nutrient supply in cartilage tissue engineering. *Biotechnology Progress*, *21*, 1252–1261. https://doi.org/10.1021/bp0500157

Skrzypek, K., Nibbelink, M. G., Karbaat, L. P., Karperien, M., van Apeldoorn Apeldoorn, A., & Stamatialis, D. (2018). An important step towards a prevascularized islet macroencapsulation device-effect of micropatterned membranes on development of endothelial cell network. *Journal of Materials Science*, *29*, 91. 15pp. https://doi.org/10.1007/s10856-018-6102-0

Song, K., Wang, H., Zhang, B., Lim, M., Liu, Y., & Liu, T. (2013). Numerical simulation of fluid field and in vitro three-dimensional fabrication of tissue-engineered bones in a rotating bioreactor and in vivo implantation for repairing segmental bone defects. *Cell Stress and Chaperones*, *18*, 193–201. https://doi.org/10.1007/s12192-012-0370-2

Song, K., Yan, X., Zhang, Y., Song, F., Lim, M., Fang, M., … Liu, T. (2015). Numberical simulation of fluid flow and three-dimensional expansion of tissue engineering seed cells in large scale inside a novel rotating wall hollow fiber membrane bioreactor. *Bioprocess and Biosystems Engineering*, *38*, 1527–1540. https://doi.org/10.1007/s00449-015-1395-6

Spencer, T. J., Hidalgo-Bastida, L. A., Cartmell, S. H., Halliday, I., & Care, C. M. (2013). In silico multi-scale model of transport and dynamic seeding in a bone tissue engineering perfusion bioreactor. *Biotechnology and Bioengineering*, *110*, 1221–1230. https://doi.org/10.1002/bit.24777

Stamatialis, D. (2017). Bioartificial organs and tissue engineering. *International Journal of Artificial Organs*, *40*, 133–135. https://doi.org/10.5301/ijao.5000599

Waller, B. F., Orr, C. M., Slack, J. D., Pinkerton, C. A., Van tassel tassel, J., & Peters, T. (1992). Anatomy, histology, and pathology of coronary arteries: A review relevant to new interventional and imaging techniques-part I. *Clinical Cardiology*, *15*, 451–457. https://doi.org/10.1002/clc.4960150613

Zhao, F., Vaughan, T. J., & Mcnamara, L. M. (2015). Multiscale fluid–structure interaction modeling to determine the mechanical stimulation of bone cells in a tissue engineered scaffold. *Biomechanics and Modeling in Mechanobiology*, *14*, 231–243. https://doi.org/10.1007/s10237-014-0599-z

Zhu, G.-C., Gu, Y.-Q., Geng, X., Feng, Z. G., Zhang, S. W., Ye, L., & Wang, Z. G. (2015). Experimental study on the construction of small three-dimensional tissue engineered grafts of electrospun poly-epsilon-caprolactone. *Journal of Materials Science*, *26*, 16. https://doi.org/10.1007/s10856-015-5448-9. pp

Zhu, Y., Song, K., Jiang, S., Chen, J., Tang, L., Li, S., … Liu, T. (2017). Numerical simulation of mass transfer and three-dimensional fabrication of tissue-engineered cartilages based on chitosan/gelatin hybrid hydrogel scaffold in a rotating bioreactor. *Applied Biochemistry and Biotechnology*, *181*, 250–266. https://doi.org/10.1007/s12010-016-2210-9

How to cite this article: Elsayed Y, Lekakou C, Tomlins P. Modeling, simulations, and optimization of smooth muscle cell tissue engineering for the production of vascular grafts. *Biotechnology and Bioengineering*. 2019;116:1509–1522. https://doi.org/10.1002/bit.26955